RAPID COMMUNICATION

The design and preparation of a Fabry–Pérot polarizing filter*

Hou Yong-Qiang(侯永强)[a)b)], Qi Hong-Ji(齐红基)[a)†], and Yi Kui(易 葵)[a)]

[a)] Key Laboratory of Materials for High Power Laser, Shanghai Institute of Optics and Fine Mechanics, Chinese Academy of Sciences, Shanghai 201800, China
[b)] Shanghai Huali Microelectronics Corporation, Shanghai 201203, China

(Received 30 April 2013; revised manuscript received 13 June 2013)

A novel single-cavity narrowband Fabry–Pérot (FP) polarizing filter at normal incidence, constructed from a sandwich structure with sculptured anisotropic space layer and symmetric isotropic HR mirrors, is designed and prepared. The optical performances of transmittance, phase shift, central wavelength, and bandwidth for two polarized states are analyzed with the characteristic matrix. The numerical studies accord reasonably well with the experimental results. It is demonstrated that the polarization state of the electromagnetic wave and phase shift can be modulated by employing an anisotropic space layer in the polarizing beam splitter system. The birefringence of the anisotropic space layer provides a sophisticated phase modulation by varying the incidence angles over a broad range to have a wide-angle phase shift.

Keywords: Fabry–Pérot filter, birefringence, thin films, optical properties

PACS: 78.20.Fm, 78.20.Ci, 42.25.Ja **DOI:** 10.1088/1674-1056/22/10/107801

1. Introduction

A notch filter is one that highly transmits all the incident waves over a given transmission band and reflects other wavelengths elsewhere. Owing to superior optical and mechanical properties, including efficient suppression of higher frequency harmonics, higher laser-induced damage threshold, smaller residual stress, higher scratch, and wear resistance, the FP filter has received considerable attention for optical components and applications such as tunable filters,[1,2] optical interference filters,[3,4] Bragg grating filters,[5,6] rugate filters,[7,8] etc. In contrast to conventional all-dielectric optical filters constructed from isotropic thin films, filters designed with three-dimensional (3D) nanostructured sculptured anisotropic thin films[9] (ATFs) prepared via the glancing angle deposition (GLAD) technique can perform better in manipulating the polarization state of electromagnetic waves because the ATF presents birefringence. This property is very important for the development of polarization and phase components for the miniaturization of integrated optical systems.

In this paper, because of a large bulk refractive index, good mechanical and thermal stability, high static dielectric constant, and excellent transparency at visible wavelengths, we investigate the feasibility of employing a TiO_2 anisotropic space layer with highly orientated microstructure composed of slanted nanocolumns for a high-efficiency FP polarizing filter. The optical performances of the transmittance, phase shift, central wavelength, and bandwidth for two polarized states are theoretically analyzed with the characteristic matrix and experimentally characterized with spectrophotometry and scanning electron microscopy. The results demonstrate that the polarization state of electromagnetic wave and phase shift can be modulated by selecting an appropriate birefringence of the ATF and incidence angle of the polarized wave. Birefringence of the biaxial ATF provides a sophisticated phase modulation by varying incidence angles over a broad range to have a wide-angle phase shift.

2. Design of FP polarizing filter

The basic single-cavity narrowband FP polarizing filter comprises quarter-wave isotropic layers of alternating high and low refractive indices and half-wave biaxial anisotropic space layer, denoted as H, L, and 2N, respectively. The stacked formula layer structure is of substrate/$(HL)^5$H 2N $(HL)^5$ H/air and the phase thickness values of H, L, and N layers are all $\pi/2$ at the central reference wavelength $\lambda_0 = 632.8$ nm. In our design, HfO_2 with $n_H = 1.921$ and SiO_2 with $n_L = 1.451$ are used to construct the HR mirrors for the filter. A slanted columnar TiO_2 ATF with the optical constants, including three principal refractive indices $n_1 = 1.709$, $n_2 = 1.659$, $n_3 = 1.762$, and the column angle $\beta = 39.36°$,[10] is used as the space layer. The incident medium and substrate are homogeneous, and they are isotropic air and BK7 glass, respectively. The schematic diagram of the filter is shown in Fig. 1.

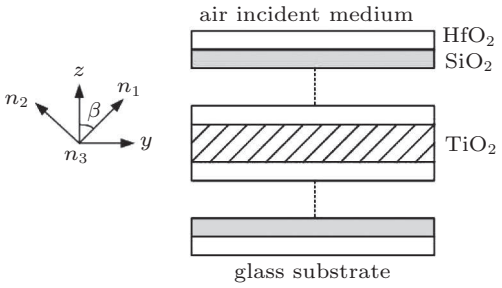


Fig. 1. Schematic plot of the single-cavity FP polarizing filter.

*Project supported by the National Natural Science Foundation of China (Grant No. 61205211).
†Corresponding author. E-mail: qhj@mail.siom.ac.cn
© 2013 Chinese Physical Society and IOP Publishing Ltd

For an isotropic all-dielectric FP filter designed as $(HL)^x$ H 2N $(HL)^x$ H, the calculations of the phase shift for two polarized states and the influence of the sample azimuth on phase shift are well known. Compared with the isotropic layers of thin films, the treatment of the ATFs is quite complicated mathematically. Even with 4×4 transmission matrices, the characteristic parameters such as the directions of wave vectors and rays, as well as the angles of refraction, could not be clearly described when the wave propagates across and through the GLAD-produced biaxial sculptured ATF in a general way. Without loss of generality, we consider the deposition plane of a biaxial ATF to be consistent with the plane of incidence, that is to say, the principal section coincides with the principal plane. In this case, the propagations of TE and TM waves are decoupled and the 4×4 matrix breaks up into two 2×2 matrixes. TE wave propagates in an ordinary manner and independent of the propagation direction. By contrast, TM wave propagates in an extraordinary manner. The forward- and backward-propagating directions of wave vectors generally differ from those of rays in birefringent thin films, thus the propagating directions of rays and wave vectors are not identical. Under the boundary continuity condition of Maxwell's equations, our previous study[11–13] has deduced the 2×2 characteristic matrices for the ordinary and extraordinary waves and they are expressed as

$$\begin{bmatrix} \cos\delta_s & \dfrac{\mathrm{i}}{\eta_s}\sin\delta_s \\ \mathrm{i}\eta_s\sin\delta_s & \cos\delta_s \end{bmatrix}$$

and

$$\frac{1}{\eta_+ + \eta_-}\begin{bmatrix} \eta_-\mathrm{e}^{\mathrm{i}\delta_+} + \eta_+\mathrm{e}^{-\mathrm{i}\delta_-} & \mathrm{e}^{\mathrm{i}\delta_+} - \mathrm{e}^{-\mathrm{i}\delta_-} \\ \eta_-\eta_+(\mathrm{e}^{\mathrm{i}\delta_+} - \mathrm{e}^{-\mathrm{i}\delta_-}) & \eta_+\mathrm{e}^{\mathrm{i}\delta_+} + \eta_-\mathrm{e}^{-\mathrm{i}\delta_-} \end{bmatrix}.$$

The characteristic matrix of the assembly can be given by

$$\begin{bmatrix} B \\ C \end{bmatrix} = M \cdot \begin{bmatrix} 1 \\ \eta_g \end{bmatrix},$$

where M is the combined characteristic matrix for ordinary and/or extraordinary wave, B and C are the normalized electric and magnetic fields at the front interface and can be used to determine the optical properties of thin films. The input optical admittance of the assembly Y is defined by $Y = C/B$. This result can be immediately extended to the general case of an assembly of n anisotropic layers (multilayer) with the principal section coincident with the principal plane. The characteristic matrix of the assembly is simply the product of the individual matrices taken in the correct order and shown as

$$\begin{bmatrix} B \\ C \end{bmatrix} = M_n M_{n-1}\cdots M_2 M_1 \begin{bmatrix} B \\ C \end{bmatrix} = M \cdot \begin{bmatrix} 1 \\ \eta_g \end{bmatrix},$$

where M_n is the characteristic matrix of the n-th layer, and the characteristic matrixes are different from each other for the two polarizations.

Just as for isotropic thin films, with the characteristic matrix relationship between TE and TM waves given above, the transmittance T, phase shift on transmission ξ and bandwidth $\Delta\lambda$ of the assembly are yielded and expressed as[14]

$$T = \frac{4\eta_0\eta_\mathrm{g}}{(\eta_0 B + C)(\eta_0 B + C)^*}, \tag{1}$$

$$\xi = \arctan\left[\frac{-Im(\eta_0 B + C)}{Re(\eta_0 B + C)}\right], \tag{2}$$

$$\Delta\lambda = \lambda_0 \frac{4\eta_\mathrm{L}^{2x+1}\eta_\mathrm{g}}{m\pi\eta_\mathrm{H}^{2x+2}}, \tag{3}$$

where m denotes the interference order of filter and n_g refers to the refractive index of emergent medium. The polarization dependence of an filter used at other than normal incidence results from Fresnel's equations. The tilted optical admittance η at an oblique angle of incidence can be shown to be equivalent to the normally incident performance and represented by

$$\eta_\mathrm{H} = n_\mathrm{H}\cdot\cos\theta_\mathrm{H}, \qquad \eta_\mathrm{L} = n_\mathrm{L}\cdot\cos\theta_\mathrm{L}$$

for TE wave and

$$\eta_\mathrm{H} = n_\mathrm{H}/\cos\theta_\mathrm{H}, \qquad \eta_\mathrm{L} = n_\mathrm{L}/\cos\theta_\mathrm{L}$$

for TM wave.

3. Preparation and characterization of FP polarizing filter

On the basis of above theoretical analysis, we prepare a single-cavity FP filter and experimentally demonstrate the feasibility of achieving a narrowband FP polarizing filter at normal incidence by employing a biaxial anisotropic space layer in the polarizing beam splitter system. The preparation details are similar to those in our previous work.[15] The spectrophotometry and scanning electron microscopy are used to characterize the optical performances of transmittance spectra and morphology of the filter. For better SEM observation, the FP filter is coated with a thin layer of n-Si (100) to improve conductivity. The cross-sectional SEM image observed by a Zeiss Auriga Field Emission Crossbeam microscope is shown in Fig. 2. The section of the sample is coincident with the deposition plane, defined as that containing the direction of column growth and substrate surface normal. As can be seen, the symmetric periodic isotropic layers of alternating high and low refractive indices and typical sculptured microstructures with highly orientated slanted nanocolumns of the space layer are observed and tend to be of optical anisotropic permittivity of the filter. Furthermore, the self-shadowing effects and limited surface diffusion mobility of obliquely deposited atoms

induce the space layer to grow with a highly porous columnar structure that slants toward the vapor flux. Pores among the nanocolumns are a significant characteristic of GLAD-produced film and the porous structure inevitably influences the optical properties for two polarized states of the filter.

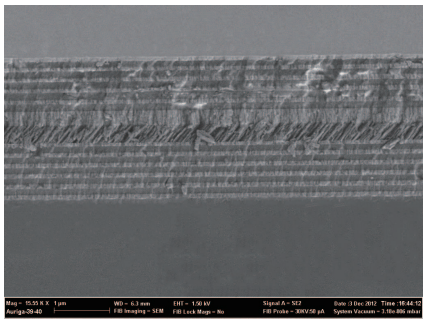


Fig. 2. Cross-sectional SEM image of our prepared single-cavity polarizing filter.

4. Results and discussion

The transmittance and phase shift spectra of the filter, performed in air from 600 nm to 660 nm at normal incidence for two polarized states, are shown in Fig. 3. Owing to the application of an anisotropic space layer in the filter, it yields different phases for TE and TM waves, and the central wavelengths for two polarizations are not overlapped, indicating that our designed FP polarizing filter at normal incidence is experimentally feasible. Numerical studies analyzed with the characteristic matrix well confirm the experimental results obtained by the Perkin–Elmer UV/VIS/NIR Lambda 1050 spectrophotometry. These findings are quite different from those obtained from the all-dielectric filter constructed with isotropic media. In addition, as for the single-cavity FP filter, the transmittance and phase shift are nearly triangular, meanwhile, the central wavelength of TE wave is longer than that of TM wave, and the peak value of phase shift is about 137° at the central wavelength.

Considering the triangular profiles of transmittance and phase shift spectra for the single-cavity filter, and one half of the energy transmitted that lies beyond the pass band, a design with two or more of the filters placed in series will be obtained with an outstanding and more close rectangular performance, furthermore, the attenuation outside the pass band is greater than that of the single filter structure. For this reason, we design a double-cavity FP polarizing filter with the stack Substrate/$(HL)^5$H 2N $(HL)^5$ H L $(HL)^5$H 2N $(HL)^5$ H/air and numerically investigate the optical properties as well as the angular-selective performances of the filter.[16] Figure 4 displays the transmittance and phase shift of the designed double-cavity filter at normal incidence. As seen in Fig. 4, the profiles of transmittance for two polarized waves are nearly rectangular and ripples are exhibited in the transmission band at the same time. In addition, the phase shift is about 284° near the central wavelength, which is almost doubled compared with that of single-cavity filter, indicating that the phase shift is approximately proportional to the physical thickness of anisotropic space layer.

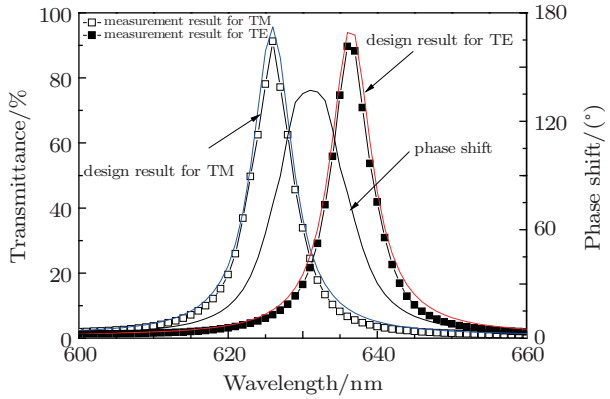


Fig. 3. (color online) Experimental results (squares) versus modeling (solid lines) results of transmittance and phase shift for two polarized states of the single-cavity filter. (The phase shifts are only given by the theoretical results derived by the characteristic matrix).

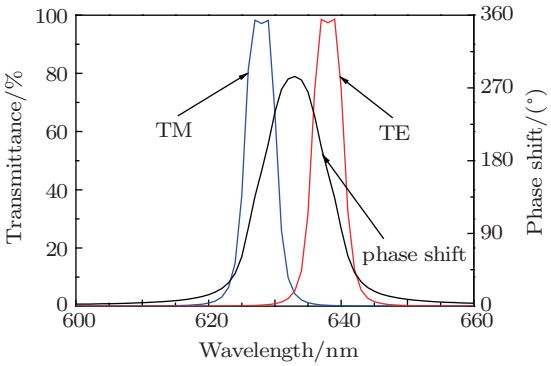


Fig. 4. (color online) Transmittances and phase shifts of the double-cavity filter for two polarizations.

The dependences of transmittance and phase shift, central wavelength, and bandwidth of the double-cavity filter on the column direction of the anisotropic space layer for two polarized states, are given in Figs. 5 and 6. For TE wave, because it propagates in an ordinary fashion with the index of refraction n_3, the central wavelength is independent of the column angle β. On the contrary, the TM wave is extraordinary, and the optical performances of the filter depend on the principal refractive indices n_1, n_2, and column angle β, thereby yielding the variable central wavelengths at different column angles. With the increase of column angle, the central wavelength shifts towards shorter wavelengths (blue-shift). The peak and valley central wavelengths are 629.6 nm and 625.2 nm for the column perpendicular and parallel to the interface of the film, respectively. In addition, the bandwidths are independent of the column angle for both TE and TM waves.

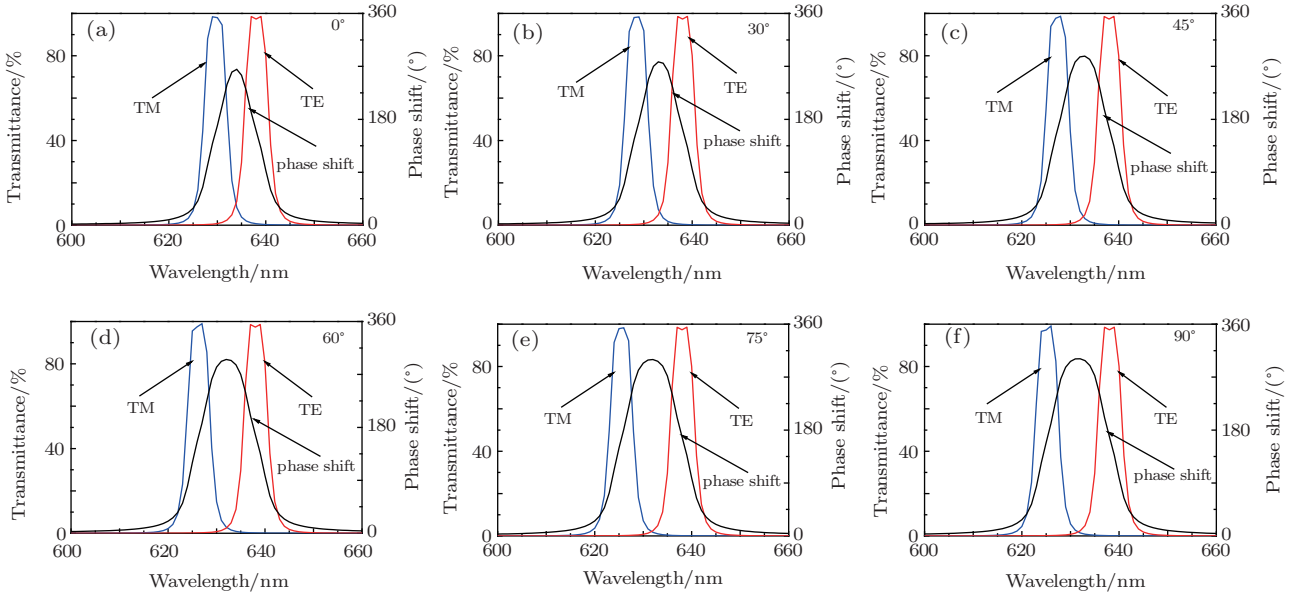


Fig. 5. (color online) Transmittances and phase shifts of the double-cavity filter with different column angles at normal incidence.

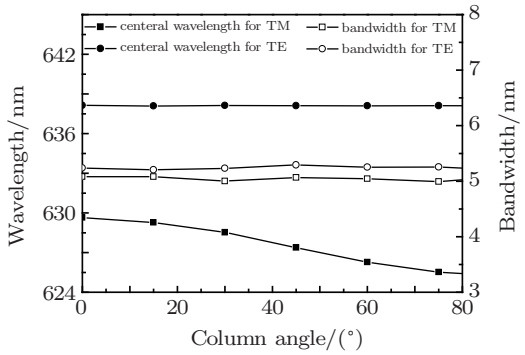


Fig. 6. Dependences of the central wavelength and bandwidth of the filter on column angle.

For oblique incidence, the tilted optical admittance and equivalent phase thickness are introduced into the analysis of optical performances of the filter. The transmittance and phase shift, central wavelength, and bandwidth of the double-cavity filter are plotted in Figs. 7 and 8 with different incidence angles of 15°, 30°, 45°, 60°, 75°, and 80°. As can be seen, as the incidence angle increases, the bandwidth of the TM wave increases accordingly, whereas that of TE wave decreases. This can be derived from Eq. (3): a higher ratio value of tilted optical admittances $\eta_{\mathrm{L}}/\eta_{\mathrm{H}}$ gives a broader band and a higher level of rejection in the stop band for a given number of periods.

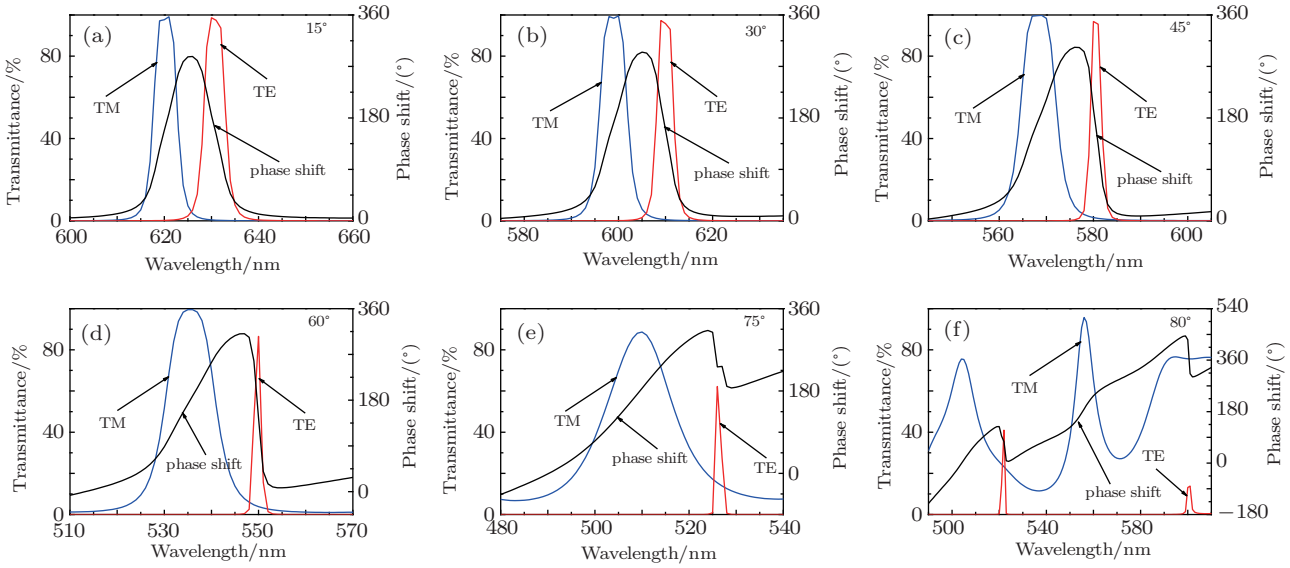


Fig. 7. (color online) Transmittances and phase shifts of the double-cavity filter at different incidence angles.

With the increase of incidence angle, the ratio of tilted optical admittances η_L/η_H increases for the TM wave, resulting in an increase of bandwidth. By contrast, the reversed trend can be obtained for the TE wave. Furthermore, an obvious modulation of the phase shift in the pass band is observed and the peak modulation depth varies from 287.5° at the incidence angle of 15° to 312.5° at the incidence angle of 75°. When the incidence angle increases to 80°, the transmission spectra of the filter are distorted severely for both TE and TM waves. In parallel, the central wavelength shifts towards shorter wavelengths for both two polarizations, and the bandwidth increases from 5.2 nm to 16.6 nm for the TM wave, whereas it decreases from 5.2 nm to 1.4 nm for the TE wave.

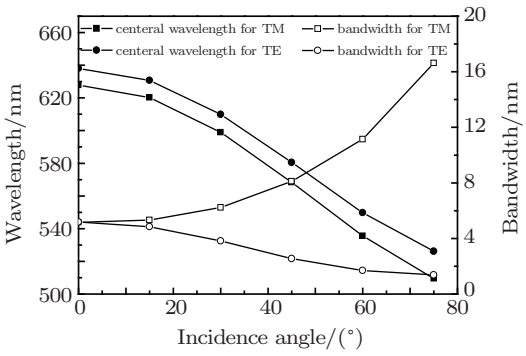


Fig. 8. Incidence angular performances of the central wavelength and bandwidth of the filter.

5. Conclusion

In the present paper, we proposed a new FP narrowband polarizing filter at normal incidence consisting of sculptured anisotropic space layer and symmetric isotropic HR mirrors and investigate the feasibility of achieving this high-efficiency filter by employing a TiO_2 anisotropic space layer with highly orientated sculptured microstructure composed of slanted nanocolumns in the polarizing beam splitter system. In contrast to a conventional all-dielectric optical filter that is constructed from isotropic layers of thin films, our designed filters can perform better in manipulating the polarization state of electromagnetic waves and phase shift because the ATF presents birefringence. Numerical studies well confirm the experimental results of the designed structure, thereby validating the model established for this kind of GLAD-produced film as well as the greater generality and superiority of characteristic matrix. Some slight deviations and drifts are mainly attributed to the idealized optical model and nanostructure confinement effects, which can affect the polarization of the ATF. In addition, the non-uniformity of our prepared tilted columnar TiO_2 ATF caused by the self-shadowing effect and the limited mobility of the deposited atoms would play a role in determining the optical properties of film interfaces and may form some space non-uniform refractive index distribution, and the spectral performance changes produced by non-uniformity are very sensitive to the incidence angle, wavelength, and polarization.[17] In this work it is demonstrated that the birefringence of the biaxial ATF provides a sophisticated phase modulation by varying incidence angles over a broad range to have a wide-angle phase shift. Furthermore, this structure can be easily used in integrated optics and we expect the design of more flexible optical components to begin in a range of anisotropic coatings.

References

[1] Sun X M, Zhou L J, Xie J Y, Zou Z, Lu L J, Zhu H K, Li X W and Chen J P 2013 *Opt. Lett.* **38** 567
[2] Yang L G, Yeh C H, Wong C Y, Chow C W, Tseng F G and Tsang H K 2013 *Opt. Express* **21** 2869
[3] Kats M A, Blanchard R, Genevet P and Capasso F 2013 *Nat. Mater.* **12** 20
[4] Hendrix K and Oliver J 2011 *Appl. Opt.* **50** 286
[5] Lumeau J, Koc C, Mokhun O, Smirnov V, Lequime M and Glebov L B 2011 *Opt. Lett.* **36** 1773
[6] Cao Y, Yang Y F, Yang X F and Tong Z R 2012 *Chin. Opt. Lett.* **10** 030605
[7] Zhang J C, Fang M, Shao Y C, Jin Y X and He H B 2011 *Chin. Phys. B* **20** 094212
[8] Zhang J C, Fang M, Shao Y C, Jin Y X and He H B 2012 *Chin. Phys. B* **21** 054219
[9] Robbie K, Brett M J and Lakhtakia A 1996 *Nature* **384** 616
[10] Hou Y Q, Qi H J, Li X, He K, Yi K and Shao J D "Phase shift of polarized light through sculptured thin films: experimental measurements and theoretical study" 2013 Chin. Phys. B (to be published)
[11] Qi H J, Zhang D P, Shao J D and Fan Z X 2005 *Europhys. Lett.* **70** 257
[12] Qi H J, Shao J D and Fan Z X 2007 *Europhys. Lett.* **78** 17004
[13] Hou Y Q, Li X, He K, Qi H J, Yi K and Shao J D 2013 *Chin. Phys. Lett.* **30** 017802
[14] Macleod H A 2010 *Thin-Film Optical Filters*, 4th edn. (Boca Rotan: CRC) pp. 13–57
[15] Qi H J, Xiao X D, He H B, Yi K and Fan Z X 2009 *Appl. Opt.* **48** 127
[16] Qi H J, Hou Y Q and Yi K 2013 *J. Opt. Soc Kor.* **17** 33
[17] Qi H J, Zhu M P, Zhang W L, Yi K, He H B and Shao J D 2012 *Chin. Opt. Lett.* **10** 013104